



## Structure–activity relationships for the interactions of 2'- and 3'-(O)-(N-methyl)anthraniloyl-substituted purine and pyrimidine nucleotides with mammalian adenylyl cyclases

Cibele Pinto<sup>a</sup>, Gerald H. Lushington<sup>b</sup>, Mark Richter<sup>c</sup>, Andreas Gille<sup>a</sup>, Jens Geduhn<sup>d</sup>, Burkhard König<sup>d</sup>, Tung-Chung Mou<sup>e</sup>, Stephen R. Sprang<sup>e</sup>, Roland Seifert<sup>f,\*</sup>

<sup>a</sup> Department of Pharmacology and Toxicology, University of Kansas, Lawrence, KS, USA

<sup>b</sup> Molecular Graphics and Modeling Laboratory, University of Kansas, Lawrence, KS, USA

<sup>c</sup> Department of Molecular Biosciences, University of Kansas, Lawrence, KS, USA

<sup>d</sup> Institute of Organic Chemistry, University of Regensburg, Germany

<sup>e</sup> Center for Biomolecular Structure and Dynamics, University of Montana, Missoula, MT, USA

<sup>f</sup> Institute of Pharmacology, Medical School of Hannover, Carl-Neuberg-Str. 1, D-30625 Hannover, Germany

### ARTICLE INFO

#### Article history:

Received 15 April 2011

Accepted 11 May 2011

Available online 18 May 2011

#### Keywords:

Adenylyl Cyclase

MANT-nucleotides

Fluorescence spectroscopy

Molecular modelling

Conformational landscape

### ABSTRACT

Membranous adenylyl cyclases (ACs) play a key role in signal transduction and are promising drug targets. In previous studies we showed that 2',3'-(O)-(N-methylanthraniloyl) (MANT)-substituted nucleotides are potent AC inhibitors. The aim of this study was to provide systematic structure–activity relationships for 21 (M)ANT-substituted nucleotides at the purified catalytic AC subunit heterodimer VC1:IC2, the VC1:VC1 homodimer and recombinant ACs 1, 2 and 5. (M)ANT-nucleotides inhibited fully activated VC1:IC2 in the order of affinity for bases hypoxanthine > uracil > cytosine > adenine ~ guanine ≫ xanthine. Omission of a hydroxyl group at the 2' or 3'-position reduced inhibitor potency as did introduction of a γ-thiophosphate group or omission of the γ-phosphate group. Substitution of the MANT-group by an ANT-group had little effect on affinity. Although all nucleotides bound to VC1:IC2 similarly according to the tripartite pharmacophore model with a site for the base, the ribose, and the phosphate chain, nucleotides exhibited subtle differences in their binding modes as revealed by fluorescence spectroscopy and molecular modelling. MANT-nucleotides also differentially interacted with the VC1:VC1 homodimer as assessed by fluorescence spectroscopy and modelling. Similar structure–activity relationships as for VC1:IC2 were obtained for recombinant ACs 1, 2 and 5, with AC2 being the least sensitive AC isoform in terms of inhibition. Overall, ACs possess a broad base-specificity with no preference for the “cognate” base adenine as verified by enzyme inhibition, fluorescence spectroscopy and molecular modelling. These properties of ACs are indicative for ligand-specific conformational landscapes that extend to the VC1:VC1 homodimer and should facilitate development of non-nucleotide inhibitors.

© 2011 Elsevier Inc. All rights reserved.

**Abbreviations:** AC, membranous adenylyl cyclase; ANT, anthraniloyl-; FRET, fluorescence resonance energy transfer; FS, forskolin; GTPγS, guanosine 5'-[γ-thio]triphosphate; MANT, methylanthraniloyl-; NDP, nucleoside 5'-diphosphate; NTP, nucleoside 5'-triphosphate; MANT-GTP, specific fluorescent nucleotides studied were: 2',3'-O-(N-methylanthraniloyl)-guanosine 5'-triphosphate; 2'-d-3'-MANT-GTP, 2'-deoxy-3'-O-(N-methylanthraniloyl)-guanosine 5'-triphosphate; 3'-d-2'-MANT-GTP, 3'-deoxy-2'-O-(N-methylanthraniloyl)-guanosine 5'-triphosphate; MANT-GTPγS, 2',3'-O-(N-methylanthraniloyl)-guanosine 5'-[γ-thio]triphosphate; MANT-ATP, 2',3'-O-(N-methylanthraniloyl)-adenosine 5'-triphosphate; 2'-d-3'-MANT-ATP, 2'-deoxy-3'-O-(N-methylanthraniloyl)-adenosine 5'-triphosphate; 3'-d-2'-MANT-ATP, 3'-deoxy-2'-O-(N-methylanthraniloyl)-adenosine 5'-triphosphate; MANT-UTP, 2',3'-O-(N-methylanthraniloyl)-uridine 5'-triphosphate; MANT-CTP, 2'/(3')-O-(N-methylanthraniloyl)-cytidine 5'-triphosphate; MANT-ITP, 2',3'-O-(N-methylanthraniloyl)-inosine 5'-triphosphate; MANT-ITPγS, 2',3'-O-(N-methylanthraniloyl)-inosine 5'-[γ-thio]triphosphate; MANT-XTP, 2',3'-O-(N-methylanthraniloyl)-xanthosine 5'-triphosphate; ANT-GTP, 2',3'-O-anthraniloyl-guanosine 5'-triphosphate; ANT-ATP, 2',3'-O-anthraniloyl-adenosine 5'-triphosphate; ANT-ADP, 2',3'-O-anthraniloyl-adenosine 5'-diphosphate; MANT-GDP, 2',3'-O-(N-methylanthraniloyl)-guanosine 5'-diphosphate; MANT-ADP, 2',3'-O-(N-methylanthraniloyl)-adenosine 5'-diphosphate; MANT-IDP, 2',3'-O-(N-methylanthraniloyl)-inosine 5'-diphosphate; MANT-UDP, 2',3'-O-(N-methylanthraniloyl)-uridine 5'-diphosphate; MANT-CDP, 2',3'-O-(N-methylanthraniloyl)-cytidine 5'-diphosphate; MANT-IMP, 2',3'-O-(N-methylanthraniloyl)-inosine 5'-monophosphate.

\* Corresponding author. Tel.: +49 511 532 2805; fax: +49 511 532 4081.

E-mail address: [seifert.roland@mh-hannover.de](mailto:seifert.roland@mh-hannover.de) (R. Seifert).

## 1. Introduction

Mammals express nine membranous AC isoforms that play an important role in signal transduction [1–3]. ACs are activated by the G-protein  $G_s$  via receptors for hormones and neurotransmitters and catalyze the production of the second messenger cAMP. ACs 1–8 are also directly activated by the diterpene, FS [1–4]. The analysis of AC knock-out mice provided important insights into the function of specific AC isoforms and potential therapeutic applications of AC inhibitors [2,5]. Currently, there is much interest in ACs 1 and 5. Specifically, AC1 knock-out mice are protected against neuronal toxicity mediated by ionotropic glutamate receptors [6,7]. AC5 knock-out mice are protected against heart failure and stress and show reduced chronic pain responses as well as increased longevity [8–11]. Thus, dual AC1/5 inhibitors may be useful drugs for the treatment of various age-related ailments including heart failure, neurodegenerative diseases, stroke and chronic pain [7,8,12].

2',3'-O-(N-Methylanthraniloyl) (MANT)-substituted nucleotides are competitive AC inhibitors [13,14]. ACs 1 and 5 are more sensitive to inhibition by MANT-nucleotides than AC2 [14]. MANT-GTP $\gamma$ S inhibits recombinant AC5 expressed in Sf9 insect cells with a  $K_i$  values of  $\sim 35$  nM [14] and blocks activation of voltage-dependent calcium channels in cardiomyocytes via AC5 [12]. Moreover, MANT-nucleotides are fluorescence probes to monitor ligand–protein interactions [15]. Upon binding of MANT-nucleotides to purified catalytic subunits of mammalian AC (C1 subunit of AC5 (VC1) and C2 subunit of AC2 (IIC2), an increase in direct fluorescence is observed, reflecting binding of the MANT-group into a hydrophobic pocket in the catalytic site [16,17]. Moreover, FRET between Trp1020 in IIC2 and the MANT-group is observed, FS increasing the signals as a reflection of optimization of the MANT binding pocket [16,17]. However, it should be emphasized that VC1:IIC2 is only a general model for membranous ACs and not a specific model for a given AC isoform. The problem is that the VC2- and IIC1 subunits are difficult to express. We tried this already in previous studies [16,17], but we failed.

Enzymatic, fluorescence spectroscopy, crystallographic and molecular modelling studies showed that ACs exhibit a high degree of conformational flexibility, allowing the catalytic site to accommodate structurally diverse bases [13,14,18–21]. Even the VC1:VC1 homodimer, although exhibiting only exceedingly low catalytic activity, is capable of binding MANT-GTP with high affinity [22]. It is possible that *in vivo*, C1:C1 dimers form through interaction of the C1-subunits of neighboring AC molecules, ensuring low basal AC activity and hence, providing a novel site for pharmacological intervention [22].

The aim of our present study was to provide a systematic structure–activity relationship of a series of 21 (M)ANT-nucleotides for VC1:IIC2 in terms of inhibition of catalysis, fluorescence spectroscopy and molecular modelling. As basis for molecular modelling, the crystal structures of VC1:IIC2 in complex with MANT-GTP, MANT-ATP and MANT-ITP are now available [16,17,23]. Moreover, we studied the properties of (M)ANT-nucleotides in terms of inhibition of recombinant ACs 1, 2 and 5 expressed in Sf9 insect cells. Finally, we analyzed the nucleotide-binding properties of the VC1:VC1 homodimer in terms of fluorescence spectroscopy and modelling. A detailed understanding of the structure–activity relationship of nucleotides for the interaction with various ACs is essential for the future development of AC isoform-selective non-nucleotide inhibitors that could be used as potential drugs.

Fig. 1 shows the structures of the nucleotides examined herein. In 2',3'-MANT-nucleotides, the MANT-group spontaneously isomerizes between the 2'- and 3'-group [15], but in the VC1:IIC2 crystal structures, the 3'-MANT isomers are favored [16,17,23].

Therefore, we also studied the defined 2'-d-3'-MANT- and 3'-d-2'-MANT-isomers of MANT-GTP (2 and 3) and MANT-ATP (6 and 7). These isomer pairs for MANT-ATP and MANT-GTP have provided valuable insights into ligand–protein interaction for a bacterial AC toxin, edema factor, from *Bacillus anthracis* [24]. Note, that in comparison to 2',3'-MANT-nucleotides, the defined 2'- and 3'-MANT-isomers lack a hydroxyl group that may be important for hydrogen bonding with AC. Moreover, we studied MANT-ITP (8), the most potent AC inhibitor known so far [21,23], differing from MANT-GTP (1) only by the lack of an  $NH_2$ -group at C2 of the purine ring. For comparison, we also studied MANT-XTP (10), bearing a keto group at C2 and inhibiting VC1:IIC2 much less potently than MANT-GTP [17,23]. Considering the relatively high potency of 2',3'-O-(2,4,6-trinitrophenyl)-UTP and 2',3'-O-(2,4,6-trinitrophenyl)-CTP for VC1:IIC2 ( $K_i$ ,  $\sim 100$ – $300$  nM range) [17] and ACs 1, 2 and 5 ( $K_i$ ,  $\sim 10$ – $100$  nM) [20], we examined the interaction of VC1:IIC2 with MANT-UTP (11) and MANT-CTP (12) as well. ANT-nucleotides differ from MANT-nucleotides by the lack of the methyl group at the anthraniloyl ring (Fig. 1) and were used for the fluorescence analysis of various proteins [15]. Therefore, we included various ANT-nucleotides (13–15, 21) into our studies as well. Finally, the length of the polyphosphate tail critically determines the affinity of AC for 2',3'-substituted nucleotides [14]. Hence, we examined several (M)ANT-NDPs (15–19) and (M)ANT-NMPs (20, 21), too.

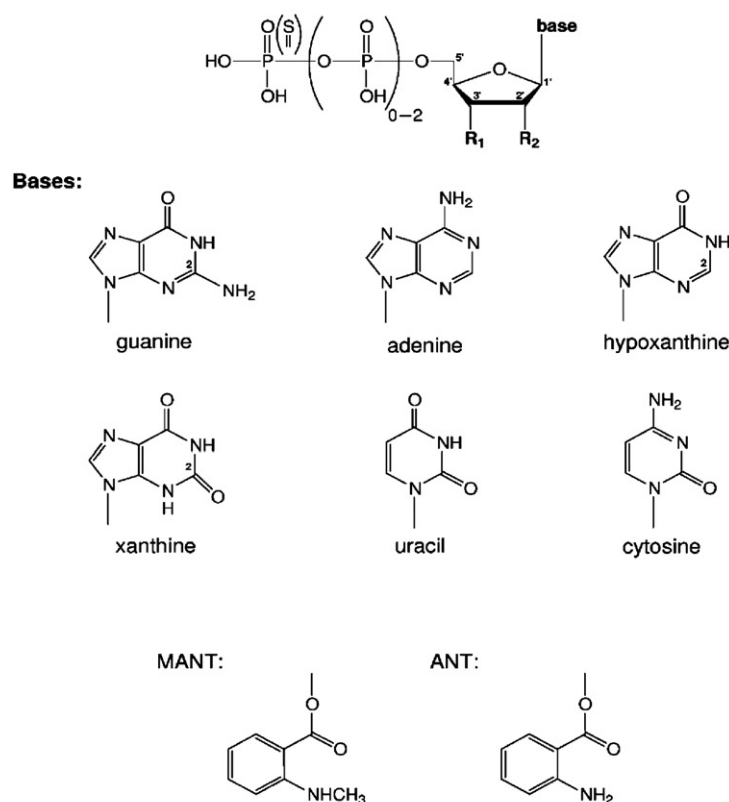
## 2. Materials and methods

### 2.1. Materials

MANT- and ANT-substituted nucleotides 8, 11, 12, 14, 15 and 17–21 were synthesized according to Hiratsuka [25] with the previously described modifications [26,27]. MANT-GTP (1), 2'-d-3'-MANT-GTP (2), 3'-d-2'-MANT-GTP (3), MANT-GTP $\gamma$ S (4), MANT-ATP (5), 2'-d-3'-MANT-ATP (6), 3'-d-2'-MANT-ATP (7), MANT-ITP $\gamma$ S (9), MANT-XTP (10), ANT-GTP (14) and MANT-ADP (16) were obtained from Jena Bioscience (Jena, Germany). Catalytic AC subunits VC1 and IIC2 and GTP $\gamma$ S-activated  $G_{s\alpha}$  ( $G_{s\alpha}$ -GTP $\gamma$ S) were expressed and purified as described [28]. [ $\alpha$ - $^{32}P$ ]ATP (800 Ci/mmol) was purchased from PerkinElmer (Wellesley, MA, USA). Aluminum oxide 90 active, neutral (activity 1, particle size 0.06–0.2 mm) was purchased from Merck (Darmstadt, Germany). Bovine serum albumin, fraction V, highest quality, was from Sigma-Aldrich (St. Louis, MO, USA).  $MnCl_2$  tetrahydrate (highest quality) was from Merck. FS was from LC Laboratories (Woburn, MA, USA).

### 2.2. Cell culture and membrane preparation

Cell culture and membrane preparation were performed as previously described [29]. Briefly, Sf9 cells were cultured in SF 900 II medium supplemented with 5% (vol/vol) fetal bovine serum and 0.1 mg/ml gentamicin. High-titer baculoviruses for ACs 1, 2 and 5 were generated through two sequential amplification steps as previously described [14,29]. In each amplification step the supernatant fluid was harvested and stored under light protection at 4 °C. For membrane preparation Sf9 cells ( $3.0 \times 10^6$  cells/ml) were infected with corresponding baculovirus encoding different mammalian ACs (1:100 dilutions of high-titer virus) and cultured for 48 h. Membranes expressing each construct and membranes from uninfected Sf9 cells were prepared as described [29]. Briefly, cells were harvested and cell suspensions were centrifuged for 10 min at  $1000 \times g$  at 4 °C. Pellets were resuspended in 10 ml of lysis buffer (1 mM EDTA, 0.2 mM phenylmethylsulfonyl fluoride, 10  $\mu$ g/ml leupeptine and 10  $\mu$ g/ml benzamide, pH 7.4). Thereafter, cells were lysed with 20–25 strokes using a Dounce homogenizer. The resultant cell fragment suspension was centrifuged for 5 min



(M)ANT- nucleotides	R <sub>1</sub>	R <sub>2</sub>
1. <b>MANT-GTP</b>	MANT / OH	
2. <b>2'-d- 3'-MANT-GTP</b>	MANT	H
3. <b>3'-d-2'-MANT-GTP</b>	H	MANT
4. <b>MANT-GTP<sub>γ</sub>S</b>	MANT / OH	
5. <b>MANT-ATP</b>	MANT / OH	
6. <b>2'-d-3'-MANT-ATP</b>	MANT	H
7. <b>3'-d-2'-MANT-ATP</b>	H	MANT
8. <b>MANT-ITP</b>	MANT / OH	
9. <b>MANT-ITP<sub>γ</sub>S</b>	MANT / OH	
10. <b>MANT-XTP</b>	MANT / OH	
11. <b>MANT-UTP</b>	MANT / OH	
12. <b>MANT-CTP</b>	MANT / OH	
13. <b>ANT-GTP</b>	ANT / OH	
14. <b>ANT-ATP</b>	ANT / OH	
15. <b>ANT-ADP</b>	ANT / OH	
16. <b>MANT-ADP</b>	MANT / OH	
17. <b>MANT-IDP</b>	MANT / OH	
18. <b>MANT-UDP</b>	MANT / OH	
19. <b>MANT-CDP</b>	MANT / OH	
20. <b>MANT-IMP</b>	MANT / OH	
21. <b>ANT-IMP</b>	ANT / OH	

**Fig. 1.** Structures of 2',3'-O-ribose-modified nucleotides. Represented are the three pharmacophores contributing to the inhibitor potencies of these nucleotides, i.e. the base, the tri- or diphosphate chain and the (M)ANT group. Studied nucleotides differed from each other in the base (guanine, hypoxanthine, xanthine, adenine, uracil and cytosine),  $\gamma$ -phosphate chain substitution (phosphate or thiophosphate), phosphate chain length (5'-triphosphate, 5'-diphosphate or 5'-monophosphate analogs), ribosyl substituent (MANT or ANT), and in the position of the MANT-group (2'- and 3'-MANT).

at 500  $\times$  g and 4 °C to sediment nuclei. The cell membrane-containing supernatant suspension was transferred into 30 ml tubes and centrifuged for 20 min at 30,000  $\times$  g and 4 °C. The supernatant fluid was discarded and cell pellets were resuspended in buffer consisting of 75 mM Tris/HCl, 12.5 mM MgCl<sub>2</sub>, and 1 mM EDTA, pH 7.4. Membrane aliquots of 1 ml were prepared, stored at –80 °C and protein concentration for each membrane preparation was determined using the Bio-Rad DC protein assay kit (Bio-Rad, Hercules, CA, USA).

### 2.3. AC activity assay

AC activity in Sf9 membranes expressing ACs 1, 2 or 5 was determined essentially as described [14]. Before experiments, membranes were sedimented by a 15 min centrifugation at 4 °C and 15,000  $\times$  g and resuspended in 75 mM Tris/HCl, pH 7.4. Reaction mixtures (50  $\mu$ l final volume) contained 30  $\mu$ g of membrane protein, 40  $\mu$ M ATP/Mn<sup>2+</sup> plus 5 mM MnCl<sub>2</sub>, 100  $\mu$ M FS, 10  $\mu$ M GTP $\gamma$ S and (M)ANT-nucleotides at concentrations from 0.1 nM to 1 mM as appropriate to obtain saturated inhibition curves. Following a 2 min pre-incubation at 37 °C, reactions were initiated by adding 20  $\mu$ l of reaction mixture containing (final) 1.0–1.5  $\mu$ Ci/tube [ $\alpha$ -<sup>32</sup>P]ATP and 0.1 mM cAMP. AC assays were conducted in the absence of an NTP-regenerating system to allow for the analysis of 2',3'-substituted (M)ANT-NDPs that could otherwise be phosphorylated to the corresponding (M)ANT-NTPs [14]. For determination of *K<sub>m</sub>* values, reactions mixtures contained 20  $\mu$ M–1 mM ATP/Mn<sup>2+</sup> as substrate [14]. Reactions were con-

ducted for 20 min at 37 °C and were terminated by adding 20  $\mu$ l of 2.2 N HCl. Denatured protein was precipitated by a 1 min centrifugation at 25 °C and 15,000  $\times$  g. Sixty-five  $\mu$ l of the supernatant fluid were applied onto disposable columns filled with 1.3 g neutral alumina. [<sup>32</sup>P]cAMP was separated from [ $\alpha$ -<sup>32</sup>P]ATP by elution of [<sup>32</sup>P]cAMP with 4 ml of 0.1 M ammonium acetate, pH 7.0. Recovery of [<sup>32</sup>P]cAMP was ~80% as assessed with [<sup>3</sup>H]cAMP as standard. [<sup>32</sup>P]cAMP was determined by Čerenkov radiation.

For experiments with purified catalytic AC subunits, reaction mixtures contained 100  $\mu$ M ATP/Mn<sup>2+</sup>, 10 mM MnCl<sub>2</sub> and (M)ANT-nucleotides at concentrations from 0.1 nM to 1 mM as appropriate to obtain saturated inhibition curves. Additionally, assay tubes contained VC1 (8 nM) and IIC2 (40 nM). For experiments with G<sub>S $\alpha$</sub> -GTP $\gamma$ S, tubes contained VC1 (3 nM), IIC2 (15 nM) and G<sub>S $\alpha$</sub> -GTP $\gamma$ S (51 nM). We have used the 1:5 ratio of VC1:IIC2 in all of our previous studies to ensure that all available VC1 molecules find a IIC2 partner [see e.g. 14, 16 and 17]. The formation of IIC2 dimers is not problematic because these dimers neither bind nucleotides nor FS and do not exhibit catalytic activity [22]. Moreover, the VC1 homodimer exhibits only exceedingly low catalytic activity [22]. Thus, under the conditions chosen, we almost exclusively analyze the VC1:IIC2 heterodimer. Reactions were conducted in the presence of 100  $\mu$ M FS. Following a 2 min pre-incubation at 30 °C, reactions were initiated by adding 20  $\mu$ l of reaction mixture containing (final) 1.0  $\mu$ Ci/tube [ $\alpha$ -<sup>32</sup>P]ATP, 0.1 mM cAMP and 100 mM KCl in 25 mM HEPES/NaOH, pH 7.4. AC assays were conducted in the absence of an NTP-regenerating system to allow

for the analysis of 2',3'-substituted (M)ANT-NDPs that could otherwise be phosphorylated to the corresponding (M)ANT-NTPs [14]. Reactions were conducted for 10–20 min at 30 °C. Competition isotherms were analyzed by non-linear regression using the Prism 4.0 software (GraphPad, San Diego, CA, USA).

#### 2.4. Fluorescence spectroscopy

All experiments were conducted using a Cary Eclipse fluorescence spectrophotometer equipped with a Peltier-thermostated multicell holder at 25 °C (Varian, Palo Alto, CA, USA). Measurements were performed in a quartz fluorescence microcuvette (Hellma, Plainview, NY, USA). The final assay volume was 150  $\mu$ l. Reaction mixtures contained a buffer consisting of 100 mM KCl, 10 mM  $\text{MnCl}_2$  and 25 mM HEPES/NaOH, pH 7.4. Steady-state emission spectra were recorded at low speed with  $\lambda_{\text{ex}} = 350$  nm ( $\lambda_{\text{em}} = 370$ –500 nm) and  $\lambda_{\text{ex}} = 280$  nm ( $\lambda_{\text{em}} = 300$ –500 nm) with various (M)ANT-nucleotides (1  $\mu$ M each) in the absence and presence of 5  $\mu$ M VC1 plus 25  $\mu$ M IIC2 without and with 100  $\mu$ M FS. We have used a 1:5 ratio of VC1:IIC2 in all of our previous studies to ensure that all available VC1 molecules find a IIC2 partner [see e.g. 14, 16 and 17]. The formation of IIC2 dimers is not problematic because these dimers neither bind nucleotides nor FS and do not give rise to fluorescence signals [22]. Moreover, the VC1 homodimer gives rise to very different fluorescence signals than the VC1:IIC2 heterodimer [22]. Thus, under the conditions chosen, we almost exclusively analyze the VC1:IIC2 heterodimer. In experiments with VC1 alone, the protein concentration was 5  $\mu$ M, and the MANT-nucleotide concentration was 1  $\mu$ M. Fluorescence recordings were analyzed with the spectrum package of the Cary Eclipse software (Varian). Baseline fluorescence (buffer alone) was subtracted from all recordings. Figs. 2, 4 and 6 show superimposed original fluorescence recordings representative for three independent experiments with different batches of VC1 and IIC2.

#### 2.5. Molecular modelling studies

Predicted structures of MANT-GTP, MANT-ITP, MANT-ATP, MANT-UTP, MANT-CTP, MANT-XTP, ANT-GTP and ANT-ATP bound to VC1:IIC2 were generated *via* molecular simulations. The complexes were constructed from the crystal structure of VC1:IIC2 bound to MANT-GTP (PDB ID 1TL7) [16]. In each case, the new complex was constructed by editing the structure of co-crystallized ligand in SYBYL 8.0 [30] to represent the desired ligand while retaining the original atomic coordinates for all structurally conserved portions of the ligand. The full complex was then protonated using SYBYL. All ligands were assumed to have a fully anionic triphosphate tail, while the receptor valences were assumed to correspond to physiological pH, with cationic lysine and arginine residues, and anionic aspartates and glutamates. Based on these assumed valences, Gasteiger–Marsili partial charges [31] were assigned to all atoms and the system was permitted some modest relaxation *via* an 11 ps molecular dynamics simulation in SYBYL (1 ps warming from 0 to 300 K, followed by 10 ps thermal equilibration) in which the ligand and all receptor residues within 5.0 Å of the ligand were left conformationally mobile. The resulting relaxed complex structures were then optimized to within SYBYL default convergence thresholds *via* molecular mechanics.

The bound conformation of the 3'-MANT analogs was taken to correspond to the structures reported in the 2GVZ (MANT-ATP) [17] and 1TL7 (MANT-GTP) [16] crystal structures. Bound conformations for the corresponding 2'-MANT analogs were determined by sketching the structures in SYBYL 8.0 [30] and docking them into the VC1:IIC2 receptor *via* Autodock [32]. Ligand

charges were assigned *via* the Gasteiger–Marsili formalism [33], assuming a net charge state of -4, with oxygens on the  $\alpha$ - and  $\beta$ -phosphate units sharing a charge of -1 per unit, and oxygens on the  $\gamma$ -phosphate sharing a -2 charge. For all docking calculations, the receptor was prepared by removing the co-crystallized ligand and crystallographic waters from the 2GVZ crystal structure, protonating the structure in SYBYL (assuming physiological pH: cationic arginine and lysine residues; anionic aspartates and glutamates), and adding Gasteiger–Marsili charges. The docked poses for each ligand were determined to be the lowest energy conformer of the most populous cluster as observed among 100 Lamarckian genetic algorithms searches in Autodock. The resulting poses were refined in SYBYL *via* a 10 ps molecular dynamics simulation at 300 K followed by molecular mechanics optimization to full convergence according to default thresholds. In both of the latter refinement processes, all receptor atoms were held rigidly fixed, while ligand atoms were permitted to relax according to the Tripos molecular force field [34] and Gasteiger–Marsili electrostatics.

To generate the VC1:VC1 homodimer model, the first VC1 subunit was retained as reported in the crystal structure previously reported [35], and the second VC1 subunit was mapped to the framework *via* the Modeller program [36]. Sequence alignment between the VC1 target and the IIC2 template was performed with the Custal-W program [37] using the BLOSUM-30 substitution matrix [38], and standard gap penalties of 10 for opening and 0.1 for extension. Ligand interactions with residue 1029 were quantified in SYBYL 8.0 [30] *via* the Tripos Molecular Force Field [34] and Gasteiger–Marsili electrostatics [33].

### 3. Results

#### 3.1. Inhibition of the catalytic activity of VC1:IIC2 heterodimer by (M)ANT-nucleotides

Table 1 summarizes the inhibitory effects of (M)ANT-nucleotides on the catalytic activity of VC1:IIC2. All nucleotides reduced catalysis according to monophasic sigmoidal inhibition isotherms. Defined 3'-O and 2'-O-isomers of both MANT-GTP (2, 3) and MANT-ATP (6, 7) exhibited 5–20-fold lower inhibitory potencies for the maximally stimulated VC1:IIC2 ( $\text{Mn}^{2+}$  + FS +  $\text{G}_{\text{S}\alpha\text{-GTP}\gamma\text{S}}$ ) than MANT-GTP (1) and MANT-ATP (5), respectively. 3'-d-2'-MANT-GTP (3) was two-fold less potent than the 2'-d-3'-MANT derivative (2). Although previous studies showed that MANT-ATP also binds to VC1:IIC2 preferably as 3'-isomer [17], contrary to MANT-guanine nucleotides 1–3, 2'-d-3'-MANT-ATP (6) was less potent than the 2'-MANT-derivative (7) at inhibiting VC1:IIC2 catalytic activity. MANT-UTP (11) and MANT-CTP (12) exhibited two- to three-fold higher inhibitory potencies at VC1:IIC2 than MANT-GTP (1) and MANT-ATP (5) under maximally stimulatory conditions. In contrast to the MANT-GTP/MANT-GTP $\gamma$ S pair (1  $\rightarrow$  4), exchange of the  $\gamma$ -thiophosphate by a phosphate in hypoxanthine nucleotides increased the inhibitory potency by almost 30-fold (9  $\rightarrow$  8). Introduction of a keto group at the C2 carbon atom of the purine ring (8  $\rightarrow$  10) decreased inhibitor potency several hundred-fold. Deletion of the methyl group from the fluorophore at the 2',3'-O-ribosyl substituent in NTPs (compare 1 and 13, 5 and 14) did not largely change their affinity for VC1:IIC2 in the presence of  $\text{G}_{\text{S}\alpha\text{-GTP}\gamma\text{S}}$  (Table 1). Deletion of the  $\gamma$ -phosphate reduced the inhibitory potency of (M)ANT-NDPs  $\sim$ 10–80-fold compared to the corresponding (M)ANT-NTPs (compare 14 and 15, 5 and 16, 11 and 18, 12 and 19) (Table 1).

Under submaximally stimulatory conditions, i.e. in the absence of  $\text{G}_{\text{S}\alpha\text{-GTP}\gamma\text{S}}$ , the potencies of nucleotides were generally lower than under maximally stimulatory conditions. However, since



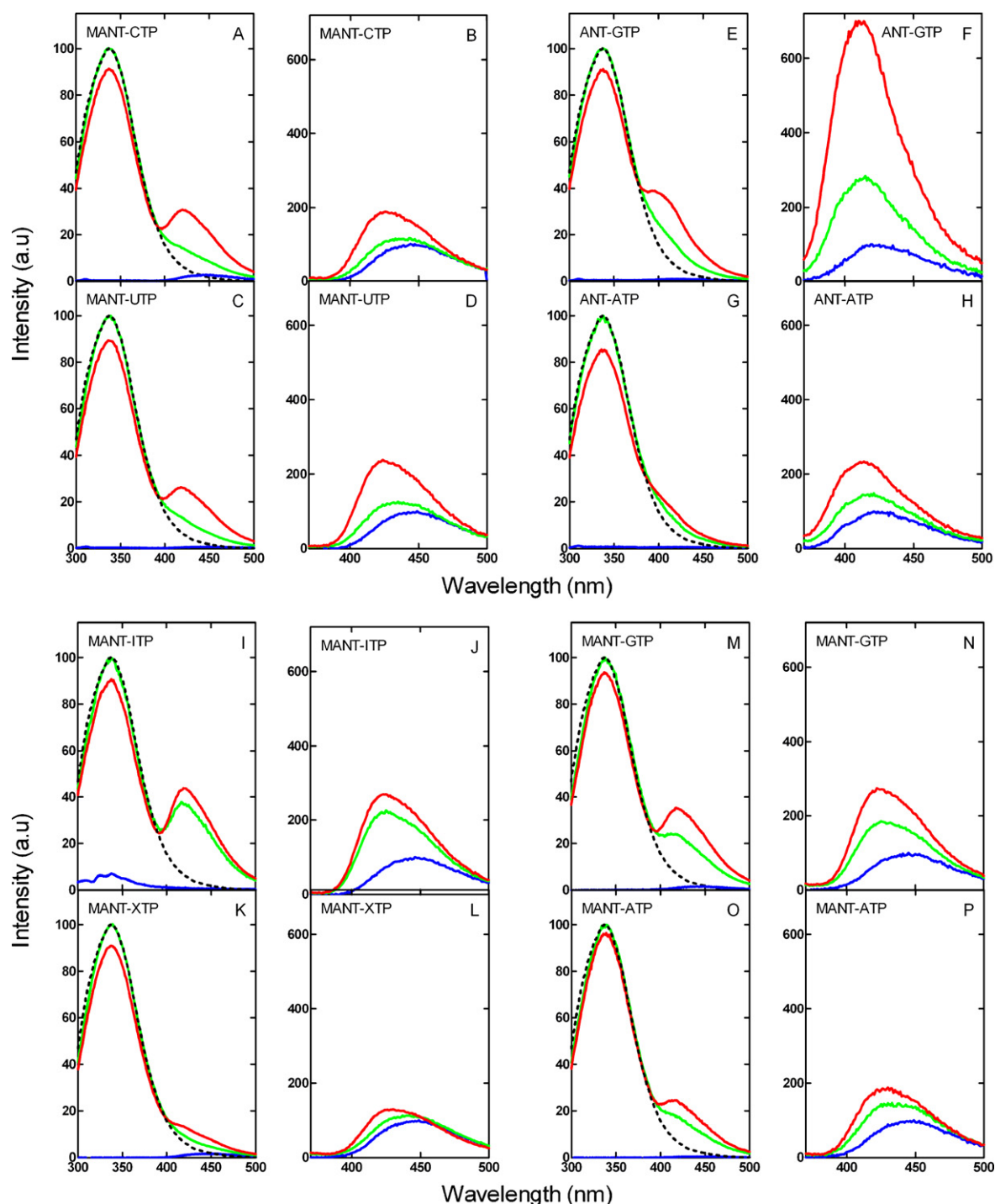


**Fig. 2.** Fluorescence emission spectra of (M)ANT-nucleotides bound to VC1:IIC2 heterodimer. Shown are representative fluorescence emission spectra of MANT-CTP, MANT-UTP, ANT-GTP, ANT-ATP, MANT-ITP, MANT-XTP, MANT-GTP and MANT-ATP at  $\lambda_{\text{ex}} = 280$  nm ( $\lambda_{\text{em}} = 300\text{--}500$  nm) (panels A, C, E, G, I, K, M and O, respectively) and at  $\lambda_{\text{ex}} = 350$  nm ( $\lambda_{\text{em}} = 370\text{--}500$  nm) (panels B, D, F, H, J, L, N and P, respectively). Experiments were conducted in the presence of different (M)ANT-nucleotides (1  $\mu\text{M}$  each), VC1 (5  $\mu\text{M}$ ) and IIC2 (25  $\mu\text{M}$ ) without FS and with FS (100  $\mu\text{M}$ ). Fluorescence measurements were performed in a quartz fluorescence microcuvette using a Cary Eclipse fluorescence spectrophotometer at 25 °C as described under “Section 2”. Reaction mixture contained 100 mM KCl, 10 mM  $\text{MnCl}_2$ , 25 mM HEPES/NaOH, pH 7.4. The final assay volume was 150  $\mu\text{l}$ , and the final DMSO concentration was 3% (vol/vol). Fluorescence intensities are shown in arbitrary units. In FRET experiments, 100% of fluorescence intensity was defined as the maximum signal obtained with VC1:IIC2 alone. In direct fluorescence experiments, 100% of fluorescence intensity was defined as the signal obtained with nucleotide alone. Fluorescence tracings are representative for two to three independent experiments with at least two different batches of VC1:IIC2. Order of addition: Blue tracings, addition of nucleotide; green tracings, addition of VC1:IIC2; red tracings, addition of forskolin. Dashed tracings, fluorescence of VC1:IIC2 alone. (For interpretation of the references to color in this figure legend, the reader is referred to the web version of this article.)

fluorescence studies with VC1:IIC2 were performed in the absence of  $G_{\text{s}\alpha\text{-GTP}\gamma\text{S}}$  (Figs. 2 and 4), it was important to determine inhibitor potencies under these experimental conditions as well. Under submaximally stimulatory conditions, potencies of nucleotides were 3.4- to 84-fold lower compared to maximally stimulatory

conditions. The affinity-difference was most pronounced for ANT-ADP (15, 84-fold) and least pronounced for 3'-d-2'-MANT-GTP (3, 3.4-fold). In the absence of  $G_{\text{s}\alpha\text{-GTP}\gamma\text{S}}$ , the order of potencies of MANT-NTPs was MANT-ITP > MANT-UTP > MANT-ATP ~ MANT-GTP > MANT-CTP  $\gg$  MANT-XTP.

**Table 1**

Inhibition of the catalytic activity of VC1:IIC2 by (M)ANT-nucleotides.

	(M)ANT-nucleotide	VC1:IIC2 $Mn^{2+}$ + FS + $G_{50\alpha}$ -GTP $\gamma$ S $K_i$ (nM)	VC1:IIC2 $Mn^{2+}$ + FS $K_i$ (nM)
1	MANT-GTP	18 ± 6.0	130 ± 20
2	2'-d-3'-MANT-GTP	180 ± 6.1	890 ± 180
3	3'-d-2'-MANT-GTP	350 ± 43	1200 ± 74
4	MANT-GTP $\gamma$ S	24 ± 4.1	N.D.
5	MANT-ATP	16 ± 6.4	100 ± 27
6	2'-d-3'-MANT-ATP	190 ± 3.4	2100 ± 160
7	3'-d-2'-MANT-ATP	90 ± 2.2	1200 ± 100
8	MANT-ITP	0.7 ± 0.1	7.0 ± 3.2
9	MANT-ITP $\gamma$ S	19 ± 3.3	N.D.
10	MANT-XTP	1200 ± 370	4600 ± 510
11	MANT-UTP	6.1 ± 1.3	58 ± 8.4
12	MANT-CTP	9.2 ± 1.5	260 ± 25
13	ANT-GTP	10 ± 1.7	160 ± 45
14	ANT-ATP	17 ± 2.4	180 ± 57
15	ANT-ADP	250 ± 12	21000 ± 1600
16	MANT-ADP	260 ± 40	2400 ± 110
18	MANT-UDP	170 ± 27	4700 ± 1200
19	MANT-CDP	140 ± 22	1500 ± 75

Catalytic activities of VC1:IIC2 were determined as described in "Section 2". Reactions were conducted in the presence of 10 mM  $MnCl_2$  and 100  $\mu$ M FS in the absence or presence of  $G_{50\alpha}$ -GTP $\gamma$ S. Data were analyzed by non-linear regression to calculate  $K_i$  values. The catalytic activity of VC1:IIC2 in the presence of  $Mn^{2+}$  + FS +  $G_{50\alpha}$ -GTP $\gamma$ S with 100  $\mu$ M ATP as substrate was  $2700 \pm 350$  nmol/mg/min and in the presence of  $Mn^{2+}$  + FS, the activity was  $300 \pm 110$  nmol/mg/min. The  $K_m$  values for VC1:IIC2 were previously reported for each experimental condition (430 and 620  $\mu$ M, respectively) [16] and were used to calculate  $K_i$  values from  $IC_{50}$  values. Data are given in nM and are the mean values  $\pm$ SD of 2–4 independent experiments performed in duplicates with at least two different batches of protein. N.D., not determined. Data for 1, 8 and 10 were taken from Ref. [23]. Data for the other nucleotides shown in the table were obtained in parallel with those for 1, 8 and 10 so that direct comparison is appropriate.

### 3.2. Analysis of the interaction of VC1:IIC2 heterodimer with (M)ANT-nucleotides by fluorescence spectroscopy

We determined the emission spectra of nucleotides at  $\lambda_{ex} = 350$  nm for direct excitation of the (M)ANT group [15], and at  $\lambda_{ex} = 280$  nm for analysis of FRET between Trp1020 in IIC2 and the (M)ANT group [16,17]. We performed fluorescence studies with a large molar excess of C1 and C2 relative to (M)ANT-nucleotides to allow for quantitative nucleotide binding to VC1:IIC2 [16,17]. At  $\lambda_{ex} = 280$  nm, (M)ANT-nucleotides were only minimally excited, whereas at  $\lambda_{ex} = 350$  nm they showed substantial intrinsic fluorescence signals with an emission peak at  $\sim 450$  nm (Fig. 2, blue tracings). The dashed black line indicates the endogenous tryptophan (and tyrosine) fluorescence of VC1:IIC2 at  $\lambda_{ex} = 280$  nm, i.e. the fluorescence in the absence of (M)ANT-nucleotide. Following the addition of VC1:IIC2, at  $\lambda_{ex} = 280$  nm, MANT-GTP exhibited a higher basal FRET signal, as revealed by a second emission peak at  $\lambda_{em} = 420$  nm, than MANT-ATP (green tracings, Fig. 2M and O). At  $\lambda_{ex} = 350$  nm, the interaction of MANT-GTP with VC1:IIC2 resulted in a two-fold higher increase in fluorescence and a "blue-shift" of the emission peak compared with MANT-ATP (green tracings, Fig. 2N and P). FS (100  $\mu$ M) increased basal FRET and direct fluorescence with MANT-GTP and MANT-ATP (red tracings), with the differences between MANT-GTP and MANT-ATP still being present. We also observed differences in both basal FRET between purine and pyrimidine nucleotides (MANT-ITP > MANT-GTP > MANT-ATP > MANT-CTP > MANT-UTP > MANT-XTP) (Fig. 2A, C, I, L, M and O). The stimulatory effect of FS on FRET followed the order MANT-CTP > MANT-UTP > MANT-GTP > MANT-ATP > MANT-ITP  $\sim$  MANT-XTP. At  $\lambda_{ex} = 350$  nm, the increase in basal fluorescence signal following the addition of VC1:IIC2 varied among the different MANT-substituted nucleotides (MANT-ITP > MANT-GTP > MANT-ATP > MANT-UTP > MANT-CTP > MANT-XTP) (Fig. 2B, D, J, L, N and P). For direct fluorescence increase by FS, the order was MANT-UTP > MANT-CTP  $\sim$  MANT-GTP > MANT-ATP  $\sim$  MANT-ITP > MANT-XTP.

As previously reported [25], ANT-GTP (Fig. 2F) and ANT-ATP (Fig. 2H) were also excited at  $\lambda_{ex} = 350$  nm, but exhibited a shorter wavelength of the emission maximum (420 nm). This difference in peak of emission can be also seen at  $\lambda_{ex} = 280$  nm, as the peak of

basal and FS-stimulated FRET is shifted to the left compared with the respective MANT-nucleotides (compare Fig. 2E and M, and G and O). As with the MANT-GTP/MANT-ATP pair, ANT-GTP and ANT-ATP showed significant differences in their emission spectra following the addition of VC1:IIC2 and FS. At  $\lambda_{ex} = 280$  nm, ANT-ATP, contrary to ANT-GTP, showed essentially no basal or FS-stimulated FRET (Fig. 2E and G). Furthermore, at  $\lambda_{ex} = 350$  nm, the addition of VC1:IIC2 and FS (100  $\mu$ M) resulted in a two-fold higher increase in ANT-GTP fluorescence compared with ANT-ATP (Fig. 2F and H). Moreover, the relative stimulatory effect of FS in the direct fluorescence assay at  $\lambda_{ex} = 350$  nm with ANT-nucleotides was about two-fold larger than with MANT-nucleotides. The stimulatory effect of FS on direct fluorescence of ANT-GTP bound to VC1:IIC2 was much greater than with any other (M)ANT-nucleotide studied and amounted to about 2.5-fold.

### 3.3. Analysis of the interaction of VC1:IIC2 heterodimer with (M)ANT-nucleotides by molecular modelling

Fig. 3 shows a model of the interactions of MANT-GTP, MANT-ATP, MANT-ITP, MANT-XTP, MANT-UTP, MANT-CTP, ANT-GTP and ANT-ATP with the catalytic site of VC1:IIC2 based on the crystal structure of VC1:IIC2 in complex with MANT-GTP [16]. We predict that MANT-XTP and MANT-ITP share very similar binding modes with the originally co-crystallized MANT-GTP, characterized by strong H-bonding between the base and the side chains of Lys 839 and Asp 1018 within the base-binding subpocket (Fig. 3A). In comparing ANT-GTP and MANT-GTP (Fig. 3B), essentially no significant difference is predicting in the binding conformation. However ANT-ATP is predicted to adhere to a substantially different binding mode than MANT-ATP, courtesy of a reorientation of the F400 ring that enables the ANT-group to occupy space that was not available to the other ligands. In accordance with this model, we did not observe significant basal or stimulated FRET with MANT-ATP (Fig. 2G), a finding that is in clear contrast to the data obtained for ANT-ATP (Fig. 2O), MANT-GTP (Fig. 2M) and ANT-GTP (Fig. 2E).

MANT-ATP and MANT-UTP engage in some H-bonding with this subpocket, but are predicted to be appreciably weaker in their interactions (Fig. 3A and C). For MANT-UTP, this weaker H-bonding permits the ligand to achieve stronger lipophilic interactions

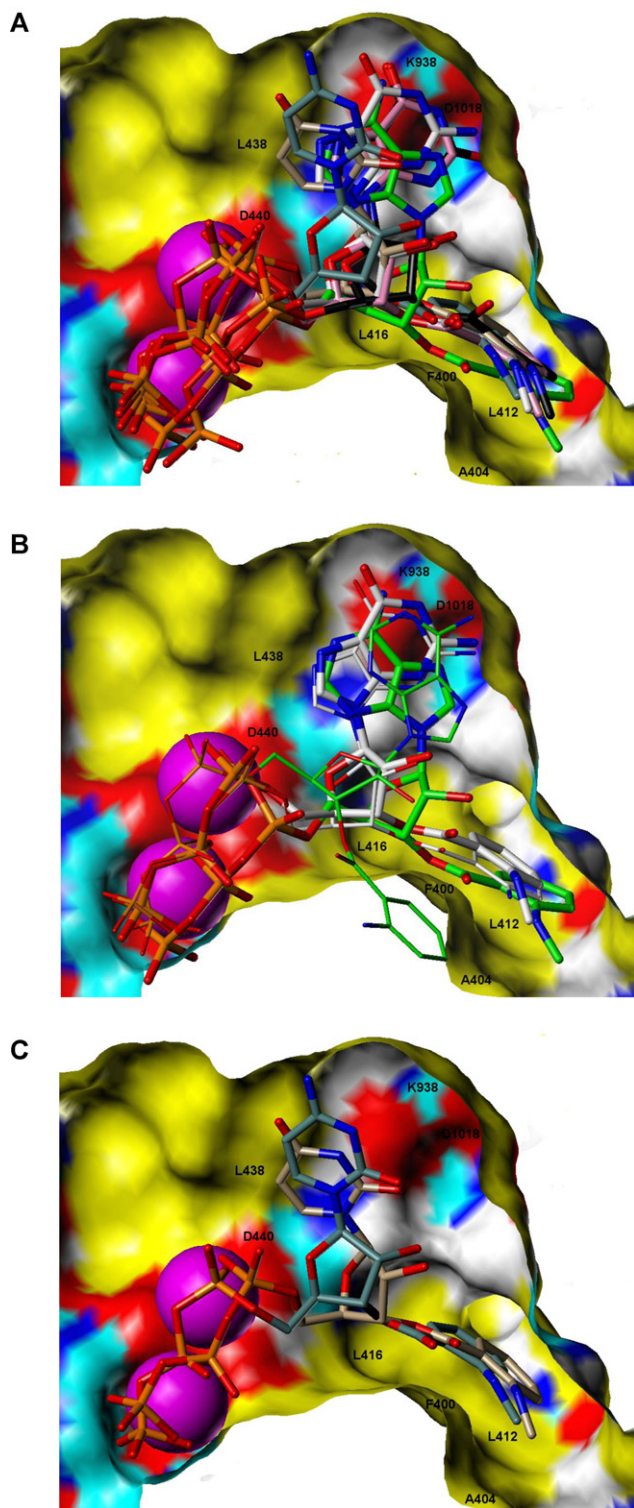


**Fig. 3.** Model of the interaction of VC1:IIC2 heterodimer with (M)ANT-nucleotides. Computationally predicted conformations for (MA)NT nucleotides bound to VC1:IIC2 comparing (A), all MANT-nucleotides; (B) (M)ANT-ATP versus (M)ANT-GTP; and (C) MANT-CTP versus MANT-UTP. Atoms of each ligand are represented as sticks (MANT ligands are thick sticks; ANT are thin) according to standard CPK coloring, except for carbon atoms which are colored as follows: (M)ANT-GTP = grey, (M)ANT-ATP = green, MANT-CTP = slate blue, MANT-ITP = black, MANT-UTP = brown, MANT-XTP = pink. The receptor surface is represented as a solvent-accessible Connolly surface, colored as follows: lipophilic regions are yellow, polar oxygens are red, polar nitrogens are blue, donatable protons are cyan, and polarized alkyl or aryl moieties are white. Approximate locations of the alpha carbons of key residues are labeled for reference. (For interpretation of the references to color in this figure legend, the reader is referred to the web version of this article.)

between the non-polar ( $-\text{CH}=\text{CH}-$ ) portion of the base and the receptor hydrophobic pocket around Leu438. MANT-CTP is predicted to completely forgo base H-bonding interactions in favor of a combination of ethylene–Leu438 interactions similar to MANT-UTP plus stronger lipophilic coupling between the MANT-group and the receptor hydrophobic pocket. Specifically, for MANT-CTP, the MANT aryl group interacts closely with Leu412, Leu416 and Trp1020 (above the plane of thus not shown), the methyl on the MANT methyl amine group has a favorable interaction with Ala404, and the methyl amine proton donates an H-bond to the side chain carbonyl-O of Asn 1025 (above plane), whereas for all other ligands the MANT group has substantially less stabilization. The stronger hydrophobic interactions of MANT-CTP with the hydrophobic pocket translated into a larger FRET signal compared to MANT-UTP (Fig. 2A and C).

#### 3.4. Analysis of the interaction of VC1:IIC2 heterodimer with 2'- and 3'-MANT-nucleotides by fluorescence spectroscopy

The overall basal fluorescence signals of VC1:IIC2 bound to 2'-d-3'-MANT-GTP and 3'-d-2'-MANT-GTP were similar to the signals of VC1:IIC2 in complex with MANT-GTP (compare Fig. 4A, E and I, as well as B, F and J), but the magnitude of FS-stimulated FRET signals at  $\lambda_{\text{ex}} = 280 \text{ nm}$  was higher with the defined isomers (2'-d-3'-MANT-GTP and 3'-d-2'-MANT-GTP) than with MANT-GTP. With adenine nucleotides, the position of the ribosyl-substituent had a very different impact on the conformations of VC1:IIC2 stabilized by these nucleotides than with guanine nucleotides (Fig. 4C, D, G, H, K and L). 3'-d-2'-MANT-ATP showed a particularly large basal FRET and direct fluorescence (Fig. 4 G and H). Unexpectedly, FS (100  $\mu\text{M}$ ) decreased FRET and direct fluorescence with 3'-d-2'-MANT-ATP. In contrast, the basal FRET and direct fluorescence increase by VC1:IIC2 with 2'-d-3'-MANT-ATP was small as was the stimulatory effect of FS (Fig. 4K and L).

#### 3.5. Analysis of the interaction of VC1:IIC2 heterodimer with 2'- and 3'-MANT-nucleotides by molecular modelling

There are three families of potentially justifiable conformers for the 2'-MANT analogs: (i) Close analogs to the 3'-MANT conformation, but with the MANT ring flipped (Fig. 5). (ii) Poses, where the binding site of the 2'-MANT group and the nucleotide are switched (not shown). (iii) Poses, where the nucleotide maintains its binding site, but the 2-MANT group couples instead with lipophilic groups on FS (not shown). Although we here only show the poses from family (i), the poses from families (ii) and (iii) were computed as having fairly comparable docking free energies. Thus, additional ligand conformations cannot be excluded. This may be particularly the case for 3'-d-2'-MANT-ATP, since in this case, in contrast to all other nucleotides, FS did not increase FRET and direct fluorescence signals, but rather decreased fluorescence (Fig. 4G and H). It is clear that the positioning of the nucleotides in the receptor is similar. Yet, it is also evident that there are subtle differences in the positioning of the MANT-group with the different isomers, fitting to the different fluorescence signals and  $K_i$  values.

#### 3.6. Analysis of the interaction of VC1:VC1 homodimer with 2'- and 3'-MANT-nucleotides by fluorescence spectroscopy

The basal FRET and direct fluorescence signals determined for the interaction of VC1:VC1 with MANT-GTP were similar as for the interaction of VC1:IIC2 with MANT-GTP (compare Fig. 2M with Fig. 6A and Fig. 2N with Fig. 6B, respectively). However, a major difference between both experimental settings is the fact that only in the presence of IIC2 stimulatory effects of FS were observed. IIC2 alone did not show fluorescence changes upon incubation with



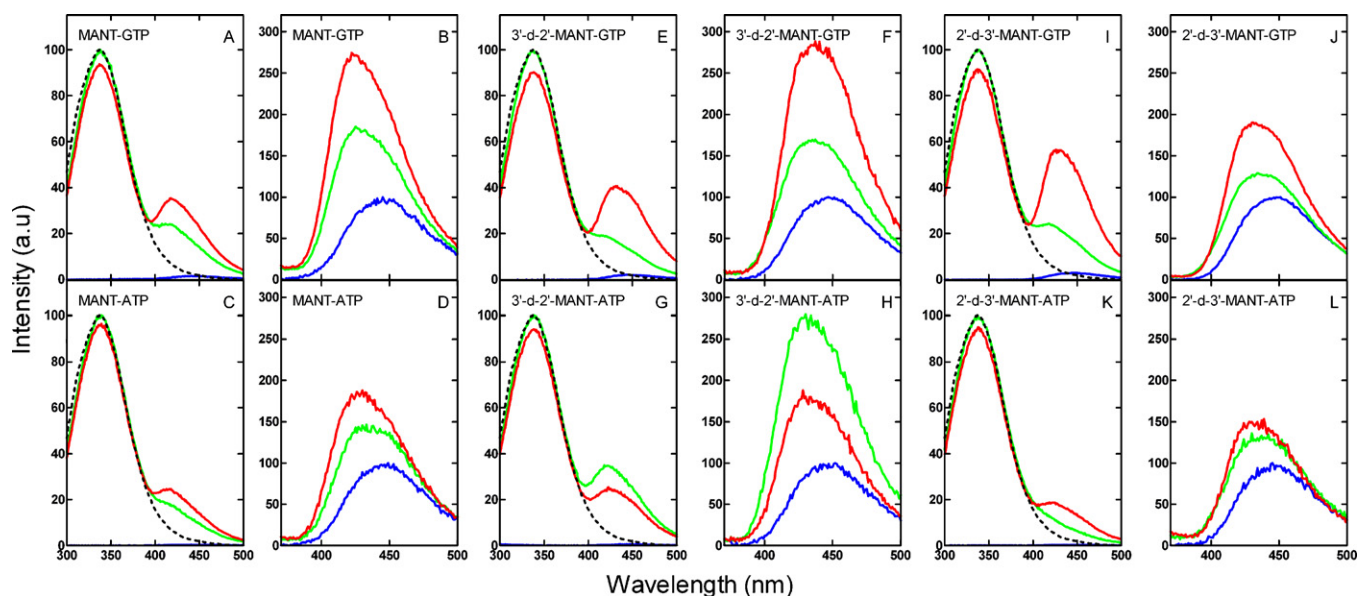


**Fig. 4.** Fluorescence emission spectra of 2'-MANT- and 3'-MANT-nucleotides bound to VC1:IIC2 heterodimer: Comparison with MANT-GTP and MANT-ATP. Shown are representative fluorescence emission spectra of MANT-GTP, MANT-ATP, 3'-d-2'-MANT-GTP, 3'-d-2'-MANT-ATP, 2'-d-3'-MANT-GTP and 2'-d-3'-MANT-ATP at  $\lambda_{\text{ex}} = 280$  nm ( $\lambda_{\text{em}} = 300\text{--}500$  nm) (panels A, C, E, G, I and K, respectively) and at  $\lambda_{\text{ex}} = 350$  nm ( $\lambda_{\text{em}} = 370\text{--}500$  nm) (panels B, D, F, H, J and L, respectively). Experiments were conducted in the presence of different MANT-nucleotides (1  $\mu\text{M}$  each), VC1 (5  $\mu\text{M}$ ) and IIC2 (25  $\mu\text{M}$ ) without FS and with FS (100  $\mu\text{M}$ ). Fluorescence measurements were performed in a quartz fluorescence microcuvette using a Cary Eclipse fluorescence spectrophotometer at 25 °C as described under "Section 2". Reaction mixture contained 100 mM KCl, 10 mM  $\text{MnCl}_2$ , 25 mM HEPES/NaOH, pH 7.4. The final assay volume was 150  $\mu\text{L}$ , and the final DMSO concentration was 3% (vol/vol). Fluorescence intensities are shown in arbitrary units. In FRET experiments, 100% of fluorescence intensity was defined as the maximum signal obtained with VC1:IIC2 alone. In direct fluorescence experiments, 100% of fluorescence intensity was defined as the signal obtained with nucleotide alone. Fluorescence tracings are representative for two to three independent experiments with at least two different batches of VC1:IIC2. Order of addition: *Blue* tracings, addition of nucleotide; *green* tracings, addition of VC1:IIC2; *red* tracings, addition of forskolin. *Dashed* tracings, fluorescence of VC1:IIC2 alone. (For interpretation of the references to color in this figure legend, the reader is referred to the web version of this article.)

MANT-nucleotides [22], indicative for the absence of a nucleotide-binding site. With VC1:VC1, we observed much larger basal FRET and direct fluorescence bound to 3'-d-2'-MANT-GTP or 2'-d-3'-MANT-GTP than with VC1:IIC2 (Fig. 6C and D versus Fig. 4E and F as

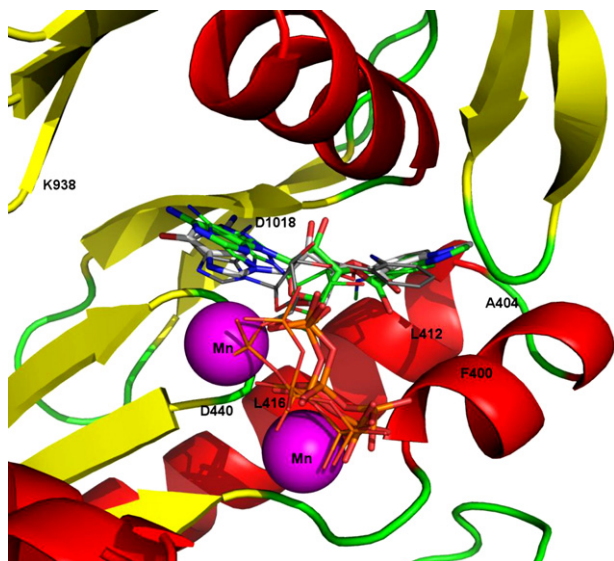
well as Fig. 6E and F versus Fig. 4I and J). Again, with the VC1 homodimer, FS failed to increase fluorescence.

Compared to basal direct fluorescence and direct FRET with VC1:IIC2 bound to MANT-ATP, the corresponding signals obtained with VC1:VC1 were much larger (compare Fig. 4C and D versus Fig. 6G and H). As was true for MANT-GTP, FS did not enhance the fluorescence signals with MANT-ATP. Similar to the observations made for VC1:IIC2, basal direct fluorescence and FRET of VC1:VC1 bound to 3'-d-2'-MANT-ATP were much larger than the signals obtained with 2'-d-3'-MANT-ATP (compare Fig. 4G and H versus Fig. 6I and J as well as Fig. 4K and L versus Fig. 6K and L). For several nucleotides, most notably 3'-d-2'-MANT-ATP, FS *reduced* the fluorescence signal with VC1:VC1.

FRET from tryptophan residues to the (M)ANT-group entails that the increase in fluorescence at the (M)ANT emission maximum at 420–450 nm should be accompanied by a corresponding decrease in fluorescence at the tryptophan fluorescence emission maximum of 350 nm [16]. However, we noticed that the extent of fluorescence decrease at  $\lambda_{\text{em}} = 350$  nm did not correlate with the increase in fluorescence at  $\lambda_{\text{em}} = 450$  nm. This was more evident in the experiments with VC1:IIC2 than in experiments with VC1:VC1 (compare Figs. 4 and 6). An explanation for these discrepancies could be that nucleotide binding to VC1:IIC2 changes the endogenous tryptophan fluorescence properties of the protein which is superimposed with the FRET signal. Changes in endogenous tryptophan fluorescence have also been observed upon nucleotide binding to signal-transducing GTP-binding proteins [39,40].

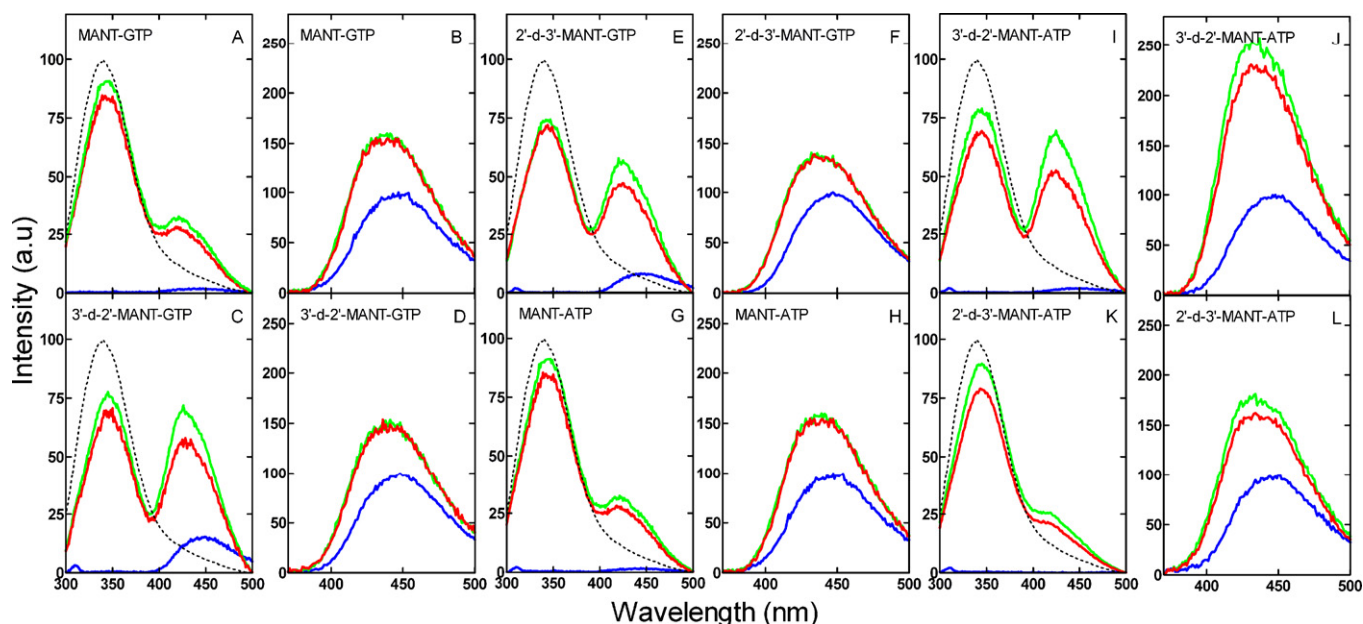
### 3.7. Analysis of the interaction of VC1:VC1 homodimer with 2'- and 3'-MANT-nucleotides by molecular modelling

Fig. 7 shows the interactions of 2'-MANT- and 3'-MANT-ATP and -GTP isomers with VC1:VC1. In the dimer, nucleotides are stabilized by hydrophobic and hydrophilic interactions. Within a distance of 3–20 Å, the MANT-group is predicted to interact with



**Fig. 5.** Model of the interaction of VC1:IIC2 heterodimer with 2'-MANT- and 3'-MANT-nucleotides. Computationally predicted conformations for the 2'-MANT- and 3'-MANT isomers of ATP and GTP bound to VC1:IIC2 are shown. The heavy sticks represent the 3'-MANT analogs (CPK atomic colors, with the molecules color codes as follows: grey carbons = MANT-GTP; green carbons = MANT-ATP) whereas the thinner sticks depict the 2'-MANT species. The AC receptor is depicted in cartoon form via red helices, yellow sheets and green coils, and the two metal cations are represented as magenta spheres. Approximate locations of the alpha carbons of key residues are labeled for reference. (For interpretation of the references to color in this figure legend, the reader is referred to the web version of this article.)





**Fig. 6.** Fluorescence emission spectra of 2'-MANT- and 3'-MANT-nucleotides bound to VC1:VC1 homodimer: Comparison with MANT-GTP and MANT-ATP. Shown are representative fluorescence emission spectra of MANT-GTP, MANT-ATP, 3'-d-2'-MANT-GTP, 3'-d-2'-MANT-ATP, 2'-d-3'-MANT-GTP and 2'-d-3'-MANT-ATP at  $\lambda_{\text{ex}} = 280$  nm ( $\lambda_{\text{em}} = 300$ –500 nm) (panels A, C, E, G, I and K, respectively) and at  $\lambda_{\text{ex}} = 350$  nm ( $\lambda_{\text{em}} = 370$ –500 nm) (panels B, D, F, H, J and L, respectively). Experiments were conducted in the presence of different MANT-nucleotides (1  $\mu\text{M}$  each) and VC1 (5  $\mu\text{M}$ ) without FS and with FS (100  $\mu\text{M}$ ). Fluorescence measurements were performed in a quartz fluorescence microcuvette using a Cary Eclipse fluorescence spectrophotometer at 25 °C as described under "Section 2". Reaction mixture contained 100 mM KCl, 10 mM  $\text{MnCl}_2$ , 25 mM HEPES/NaOH, pH 7.4. The final assay volume was 150  $\mu\text{l}$ , and the final DMSO concentration was 3% (vol/vol). Fluorescence intensities are shown in arbitrary units. In FRET experiments, 100% of fluorescence intensity was defined as the maximum signal obtained with VC1:VC1 alone. In direct fluorescence experiments, 100% of fluorescence intensity was defined as the signal obtained with nucleotide alone. Fluorescence tracings are representative for two to three independent experiments with at least two different batches of VC1:VC1. Order of addition: Blue tracings, addition of nucleotide; green tracings, addition of VC1:VC1; red tracings, addition of forskolin. Dashed tracings, fluorescence of VC1:VC1 alone. (For interpretation of the references to color in this figure legend, the reader is referred to the web version of this article.)

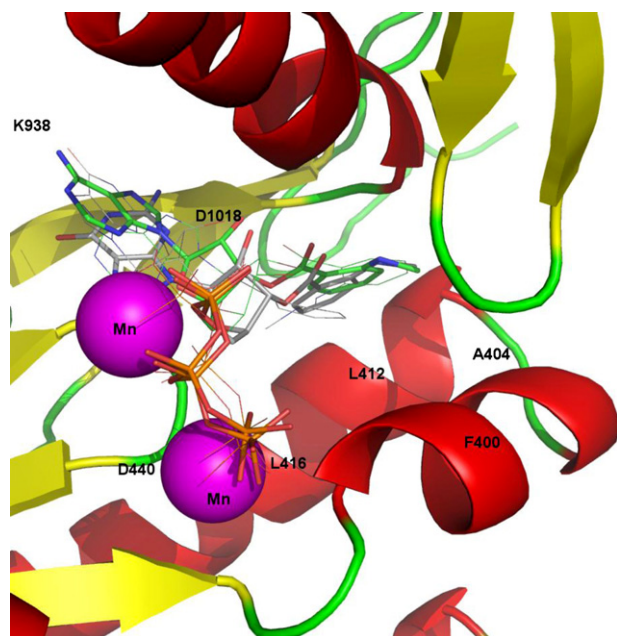


**Fig. 7.** Model of the interaction of VC1:VC1 homodimer with 2'-MANT- and 3'-MANT-nucleotides. Computationally predicted conformations for the 2'-MANT- and 3'-MANT isomers of ATP and GTP bound to VC1:VC1 are shown. The heavy sticks represent the 3'-MANT analogs (CPK atomic colors, with the molecules color codes as follows: grey carbons = MANT-GTP; green carbons = MANT-ATP) whereas the thinner sticks depict the 2'-MANT species. The AC receptor is depicted in cartoon form via red helices, yellow sheets and green coils, and the two metal cations are represented as magenta spheres. Approximate locations of the alpha carbons of key residues are labeled for reference. (For interpretation of the references to color in this figure legend, the reader is referred to the web version of this article.)

several lipophilic residues such as Ala409 and Leu413, as well as polar residues Gln410, Ser408 and Asn509. Within the same distance, the MANT-group is predicted to interact with tryptophan residues at positions 502 and 507 as well as tyrosine residues at positions 383, 442, 443, 535, 540 and 557 of VC1. These are the most likely amino acid residues contributing to the pronounced FRET and direct fluorescence signals observed for MANT-nucleotides bound to VC1:VC1, most notably 3'-d-2'-MANT-GTP (Fig. 6C), 2'-d-3'-MANT-GTP (Fig. 6E) and 3'-d-2'-MANT-ATP (Fig. 6I and J). It is evident that the positioning of the nucleotides in the receptor is similar. Yet, it is also clear that there are subtle differences in the positioning of the MANT-group with the different isomers.

### 3.8. Inhibition of the catalytic activity of recombinant ACs 1, 2 and 5 by (M)ANT-nucleotides

MANT-GTP $\gamma$ S (4) and MANT-ITP $\gamma$ S (9) were similarly potent AC5 inhibitors (Table 2). Whereas substitution of the  $\gamma$ -thiophosphate by a  $\gamma$ -phosphate had no effect on potency in case of guanine nucleotide (4  $\rightarrow$  1), this substitution increased potency in case of hypoxanthine nucleotides (9  $\rightarrow$  8) by more than 25-fold, yielding MANT-ITP. MANT-UTP was similarly potent as MANT-GTP, whereas introduction of adenine (5) or cytosine (12) decreased affinity for AC5 by 2–3-fold relative to guanine (1). Among all bases studied, xanthine (10) conferred the lowest inhibitor potency to MANT-NTPs. In case of guanine, both the 2'-d-3'-MANT-substitution (2) and the 3'-d-2'-MANT-substitution (3) substantially reduced inhibitor potency, whereas in case of adenine, only the 2'-d-3'-MANT substitution (6) decreased inhibitor potency. Exchange of the MANT-group for an ANT-group had little effect on inhibitor potency (5  $\rightarrow$  14, 15  $\rightarrow$  16 and 20  $\rightarrow$  21). Deletion of the  $\gamma$ -phosphate reduced inhibitor 5–30-

**Table 2**

Inhibition of the catalytic activity of recombinant ACs 1, 2 and 5 by (M)ANT-nucleotides.

	(M)ANT-nucleotide	AC1 (nM)	AC2 (nM)	AC5 (nM)
1	MANT-GTP	90 ± 18	610 ± 70	53 ± 12
2	2'-d-3'-MANT-GTP	270 ± 30	1300 ± 210	410 ± 35
3	3'-d-2'-MANT-GTP	1800 ± 70	8700 ± 1800	1800 ± 90
4	MANT-GTP $\gamma$ S	63 ± 17	370 ± 81	34 ± 8
5	MANT-ATP	150 ± 40	330 ± 80	100 ± 30
6	2'-d-3'-MANT-ATP	320 ± 19	4800 ± 560	360 ± 54
7	3'-d-2'-MANT-ATP	470 ± 20	540 ± 20	65 ± 5
8	MANT-ITP	2.8 ± 0.9	14 ± 0.5	1.2 ± 0.1
9	MANT-ITP $\gamma$ S	40 ± 11	120 ± 23	32 ± 8
10	MANT-UTP	1100 ± 100	3000 ± 200	1300 ± 400
11	MANT-UTP	46 ± 4.0	460 ± 60	32 ± 2.0
12	MANT-CTP	150 ± 30	690 ± 20	150 ± 30
14	ANT-ATP	130 ± 20	640 ± 70	120 ± 20
15	ANT-ADP	860 ± 10	2,900 ± 320	640 ± 70
16	MANT-ADP	1300 ± 200	2,900 ± 500	790 ± 180
17	MANT-IDP	39 ± 12	86 ± 9.1	31 ± 12
18	MANT-UDP	390 ± 50	2700 ± 300	340 ± 10
19	MANT-CDP	580 ± 10	3700 ± 420	740 ± 30
20	MANT-IMP	8500 ± 500	6800 ± 800	4400 ± 200
21	ANT-IMP	7400 ± 1200	7500 ± 1400	4300 ± 600

AC activity in Sf9 membranes was determined as described in "Section 2". Reactions were conducted in the presence of 5 mM MnCl<sub>2</sub> and 100  $\mu$ M FS. Data were analyzed by non-linear regression to calculate  $K_i$  values. The  $K_m$  values were 120  $\mu$ M (AC1), 100  $\mu$ M (AC2) and 70  $\mu$ M (AC5) and were used to calculate  $K_i$  values from  $IC_{50}$  values. Data are given in nM and are the mean values  $\pm$  SD of 4–5 independent experiments performed in duplicates with at least two different membrane preparations. Data for 5, 8 and 12, 17 and 21 were taken from Ref. [41]. Data for the other nucleotides shown in the table were obtained in parallel with those for 5, 8 and 12, 17 and 21 so that direct comparison is appropriate.

fold (5  $\rightarrow$  16, 8  $\rightarrow$  17, 11  $\rightarrow$  18 and 12  $\rightarrow$  19) and deletion of the  $\beta$ -phosphate reduced inhibitor affinity almost 150-fold (17  $\rightarrow$  20). Overall, with the exception of 3'-d-2'-MANT-ATP (7), inhibitor affinities at AC1 resembled those at AC5. Inhibitor affinities at AC2 were all lower than at ACs 1 and 5.

## 4. Discussion

### 4.1. Analysis of the VC1:IIIC2 heterodimer

The long-term goal of our group is the development of potent and isoform-specific AC inhibitors. Such inhibitors could be useful drugs for the treatment of various diseases including heart failure, chronic pain and neurodegeneration [6–12]. In order to achieve this long-term goal, a systematic analysis of the structure–activity relationships of nucleotide inhibitors is required. Accordingly, we examined 21 (M)ANT-nucleotides (Fig. 1) in terms of inhibition of catalysis (Tables 1 and 2), fluorescence spectroscopy (Figs. 2, 4 and 6) and molecular modelling (Figs. 3, 5 and 7).

Overall, our data corroborate the tripartite pharmacophore model with a site for the base, the ribose and ribosyl substituent, and the polyphosphate chain [16]. In agreement with our previous data on 2',3'-O-(2,4,6-trinitrophenyl)-substituted nucleotides [16,20], the base-specificity of VC1:IIIC2 is also very broad for 2',3'-O-MANT-substituted nucleotides with the base preference being hypoxanthine > uracil > cytosine > adenine  $\sim$  guanine  $\gg$  xanthine under maximally stimulatory conditions and the preference hypoxanthine > uracil > adenine  $\sim$  guanine > cytosine  $\gg$  xanthine under submaximally stimulatory conditions. Regardless of the experimental conditions, at least with respect to inhibitors, adenine can no longer be considered as "cognate" base for ACs.

Our studies corroborate the importance of the  $\gamma$ -phosphate for high-affinity AC inhibition [14]. Crystallographic studies showed that the Mn<sup>2+</sup> ion in the B-site coordinates with the  $\gamma$ -phosphate of MANT-nucleotides and that deletion of the  $\gamma$ -phosphate destabilizes the polyphosphate chain in its binding site [16,17]. In case of MANT-ITP and MANT-ITP $\gamma$ S, the bulky  $\gamma$ -thiophosphate impedes with coordination to the polyphosphate-binding region. In the available crystal structures, the 3'-MANT-conformation is clearly favored relative to the 2'-MANT conformation [16,17,23], but in

terms of enzyme inhibition, this is not the case, reflecting the conformational flexibility of VC1:IIIC2. The lower affinity of defined 2'- and 3'-MANT isomers for VC1:IIIC2 compared to 2',3'-MANT isomer mixtures with respect to inhibition of catalysis is explained by the absent hydrogen bond between Asn1025 of IIIC2 and the missing hydroxyl group in the defined 2'- and 3'-MANT isomers [17]. Finally, deletion of the methyl group of the MANT-substituent resulting in ANT-nucleotides (1  $\rightarrow$  13 and 5  $\rightarrow$  15) had little effect on inhibitor-affinity.

The analysis of the fluorescence signals obtained with (M)ANT-nucleotides bound to VC1:IIIC2 yielded important information on ligand/enzyme interaction. Most strikingly, the addition of FS to VC1:IIIC2 bound to 3'-d-2'-MANT-ATP reduced FRET and direct fluorescence signals (Fig. 4G and H). These data indicate that for 3'-d-2'-MANT-ATP, the hydrophobic pocket is already optimally preformed without the AC activator FS. Preparation of the corresponding crystal structure is needed to elucidate the structural basis for this unique effect. In contrast, for all all nucleotides, binding of FS to its specific interaction site optimizes interaction of the (M)ANT-group with the hydrophobic pocket adjacent to the catalytic site. These activator-dependent interactions of (M)ANT-nucleotides with VC1:IIIC2 open the possibility to develop catalysis-dependent AC inhibitors. Such compounds may be quite interesting since the therapeutic goal will probably not be to completely abrogate catalysis but only to abrogate pathologically relevant excessive catalytic activity. Another indication that this ambitious goal is achievable is the fact that full activation of VC1:IIIC2 by G<sub>SO</sub>-GTP $\gamma$ S plus FS compared to FS alone differentially increased inhibitor potencies, with the differences in potency increase differing by up to 25-fold among various compounds. In this respect, ANT-ADP (15), originally only synthesized as a rather uninformative "control compound", turned out to be the most interesting inhibitor.

The FRET and direct fluorescence signals obtained with (M)ANT-nucleotides did not correlate with inhibitor-affinity. This can be illustrated by several examples. First, MANT-GTP and MANT-ATP possess similar affinity, but the fluorescence signals with MANT-GTP were much larger than with MANT-ATP (Fig. 2M–P). A similar situation applies to the pair ANT-GTP and ANT-ATP (Fig. 2E–H). Secondly, MANT-GTP and ANT-GTP exhibit similar affinity as well, but with MANT-GTP, larger FRET signals were

obtained (Fig. 2E and M). The opposite was true for direct fluorescence signals (Fig. 2F and N). Third, 3'-d-2'-MANT-ATP shows lower affinity for VC1:IIC2 than 2'-d-3'-MANT-ATP, but larger fluorescence signals under basal conditions (Fig. 4G, H, K and L). As a last example, 3'-d-2'-MANT-GTP and 2'-d-3'-MANT-GTP possess similar affinity for VC1:IIC2, but upon exposure to FS, larger FRET signals were obtained with 2'-d-3'-MANT-GTP than with 3'-d-2'-MANT-GTP (Fig. 4E and I). These data indicate that in terms of fluorescence spectroscopy, each nucleotide imprints its specific signature on VC1:IIC2, reflecting unique positioning of any given ligand into the tripartite pharmacophore. Our molecular modelling data support this conclusion (Figs. 3 and 5). In other words, each ligand stabilizes a unique conformational landscape in VC1:IIC2 with different functional consequences. These properties of ligands and VC1:IIC2 will substantially facilitate the development of non-nucleotide-based inhibitors.

#### 4.2. Analysis of the VC1:VC1 homodimer

While the IIC2:IIC2 homodimer does not possess a functional nucleotide-binding site, the VC1:VC1 homodimer does [22,42]. Evidence for the latter notion comes for the high-affinity (although exceedingly low-efficacy) catalytic activity of VC1:VC1 and substantial fluorescence increases of MANT-GTP as well as 2',3'-O-(2,4,6-trinitrophenyl)-ATP upon binding to VC1:VC1 [22]. In this study we show that, most impressively, the basal FRET and direct fluorescence signals obtained with MANT-ATP, 3'-d-2'-MANT-ATP and 3'-d-2'-MANT-ATP largely exceed the signals obtained with the VC1:IIC2 heterodimer (Figs. 4 and 6), indicative for a formation of a binding site with better fit for the respective fluorescent nucleotides in the former receptor than in the latter one. We generated a homology model of the VC1:VC1 homodimer based on a VC1:IIC2 crystal structure [35], and this model also reveals a tripartite pharmacophore with a site for the base, a prominent hydrophobic site for the MANT-group, resulting in large FRET and fluorescence signals, and a site for the polyphosphate chain (Fig. 7). The model also shows that the MANT-groups of the different nucleotides are differentially positioned in the VC1:VC1 homodimer, again pointing to a specific conformational landscape for each nucleotide.

Intriguingly, with 3'-d-2'-MANT-ATP as probe, FS reduced fluorescence signals in the VC1:IIC2 heterodimer and the VC1:VC1 homodimer (Fig. 4G and H and Fig. 6I and J), pointing to some similarity in the interaction of the nucleotides with both receptors. In contrast to the data obtained for the heterodimer, FS reduced fluorescence signals, most notably FRET signals, in the VC1:VC1 homodimer bound to most other nucleotides. Collectively, our data show that the nucleotide-binding site formed by the VC1:VC1 homodimer possesses different regulatory properties and structure-activity relationships for nucleotides. It is conceivable that *in vivo*, C1:C1 homodimers could form through interaction of the corresponding subunits of neighboring AC molecules [22]. The function of such homodimers may be to ensure a low basal AC activity and effective stimulation of catalysis upon subsequent formation of the catalytically far more active C1:C2 heterodimer. Accordingly, the nucleotide-binding site formed by AC C1:C1 homodimers may constitute a novel regulatory site that should be considered in the future design of AC inhibitors. Blockade of the nucleotide-binding site of the C1:C1 homodimer may result in elevated basal AC activity. Whether such activity is desired or not cannot yet be answered since to this end, very little attention has been paid to the possible (patho)physiological relevance of basal AC activity. However, it is clear that AC2 possesses a particularly high basal AC activity that can be inhibited by certain FS derivatives [4,43]. Since the catalytic activity of the VC1:VC1 homodimer is so exceedingly low, the analysis of the homodimer by fluorescence spectroscopy constitutes a feasible approach to

study the newly identified nucleotide-binding site in this protein. However, it should be noted that such analysis by fluorescence spectroscopy is also not trivial since high concentrations of VC1 are required and since purification of this protein is much more difficult than purification of IIC2 both in terms of protein yield and protein stability.

#### 4.3. Analysis of recombinant holo-ACs

In accordance with previous data [14,21,22], we corroborated the generally lower sensitivity of AC2 to (M)ANT-nucleotide inhibitors compared to ACs 1 and 5. This difference can be partially explained by the Ala409Pro- and Val1108Ile exchanges in ACs 1 and 5 *versus* AC2. [16]. However, we also noted nucleotide-dependent differences in potency between the various AC isoforms. Specifically, the potency difference of MANT-GTP, MANT-UTP and 2'-d-3'-MANT-ATP amounted to >10-fold for comparison of AC5 *versus* AC2, whereas the smallest difference was observed for MANT-IMP (20) and ANT-IMP (21) (smaller than two-fold). Again, like in the case of ANT-ADP (15) and VC1:IIC2, "control compounds" of supposedly low interest, turned out to be much more informative than originally assumed. These data indicate that in principle, it should be possible to develop AC2-selective inhibitors. Such compounds should not exploit the polyphosphate-binding site and, therefore, should be of non-nucleotide structure.

Overall, the structure-activity relationships of VC1:IIC2 and holo-ACs 1, 2 and 5 are similar in terms of broad base-specificity, preference for hypoxanthine and uracil as bases and importance of the polyphosphate chain for high inhibitor affinity. However, we also noted some interesting differences between VC1:IIC2 and holo-ACs. Particularly, VC1:IIC2 did not exhibit prominent preference for 3'-MANT isomers compared to 2'-MANT-isomers in terms of potency of enzyme inhibition, although in the crystals, the 3'-MANT isomers are clearly favored [16,17,23]. However, crystals are static structures, and the catalytically active VC1:IIC2 is a conformationally flexible and "breathing" protein, largely compensating for constraints observed in static structures. In contrast, holo-ACs exhibited more marked preference for 2'-d-3'-MANT-GTP compared to 3'-d-2'-MANT-GTP. This difference was also observed for the 3'-MANT- and 2'-MANT isomers of ATP, except for AC1. These data indicate that the presence of the transmembrane domains in holo-ACs, missing in the fully soluble VC1:IIC2 system, imposes a rigidifying effect on the catalytic sites in ACs 1 and 5, and also, to a somewhat smaller extent, on AC1, increasing the expected preference of the AC isoforms for 3'-MANT isomers based on static crystal structures.

Unfortunately, nucleotides *per se* are not useful as therapeutic compounds since they do not penetrate the plasma membrane [12,44]. The design of pronucleotides, converted to the actually active compounds in intact cells, may constitute a solution to the problem [44]. Alternatively, non-nucleotide-based isoform-selective AC inhibitors may be designed. Although this goal is certainly ambitious, it is not totally elusive. This is illustrated by the case of MANT-IDP (17) and MANT-IMP (20), once again, originally thought to be "control compounds" of little interest. Usually, the deletion of the  $\beta$ - and  $\gamma$ -phosphate decreases AC inhibitor-affinity dramatically. However, MANT-IDP possesses still the same inhibitory potency as MANT-UTP (11), and the inhibitory potency of MANT-IMP is still in the low  $\mu$ M-range. Hence, provided that the base- and ribosyl-binding domains are optimally exploited with feasible structural elements, the polyphosphate-binding domain may be dispensable for inhibitor design, yielding the desired non-nucleotide compounds.

The high-affinity interactions of MANT-UTP (11) and MANT-CTP (12) with ACs are quite amazing. In fact, under certain



experimental conditions, these nucleotides even surpass MANT-ATP in terms of affinity although adenine is the “cognate” base for ACs. Previously, we had reported high-affinity interactions of 2',3'-O-(2',4',6'-trinitrophenyl)-substituted uracil- and cytosine nucleotides with various ACs. Even UTP and CTP bind to submaximally and maximally activated VC1:IIC2 with similar affinity as GTP [18]. Hence, ACs do not possess a striking specificity for the “cognate” base adenine. Collectively, all these data raise the most intriguing question whether ACs, in addition to cAMP, can also catalyze the production of cCMP and cUMP. In other words; are ACs rather purinyl- and pyrimidinyl cyclase with a broader substrate-specificity than generally assumed? In case of the highly active “AC” toxins CyaA from *Bordetella pertussis* and edema factor from *B. anthracis*, it has already recently been shown that these proteins can also catalyze the formation of cCMP and cUMP [45].

#### 4.4. Conclusions and future studies

Our present study provided a comprehensive analysis of the structure–activity relationships of (M)ANT-nucleotides for AC inhibition, analysis of the fluorescence properties of nucleotides bound to AC and molecular modelling of the interactions of (M)ANT-nucleotides with AC. Similar structure–activity relationships as for VC1:IIC2 were obtained for recombinant ACs 1, 2 and 5, with AC2 being the least sensitive AC isoform in terms of inhibition. Overall, ACs possess a broad base-specificity with no preference for the “cognate” base adenine as verified by enzyme inhibition, fluorescence spectroscopy and molecular modelling. These properties of ACs are indicative for ligand-specific conformational landscapes.

Our results yield numerous directions for future studies. First, 2'-MANT- and 3'-MANT-isomers of MANT-ITP, MANT-CTP and MANT-UTP as well as ANT-pyrimidine nucleotides, all of which have not yet been synthesized, should be examined. Second, various homologous combinations of the C1- and C2 subunits of ACs should be studied, but the expression of such functionally active subunits is not trivial. Third, the crystal structure of the VC1:VC1 homodimer bound to some of the nucleotides analyzed herein should be analyzed to better understand the structural basis for the strong basal fluorescence signals and the inhibitory effects of FS on fluorescence. Fourth, different AC isoforms than ACs 1, 2 and 5 should be examined. Again, functional expression of such isoforms in Sf9 cells is not easy. Fifth, the broad base-specificity of AC inhibitors urgently calls for a systematic analysis of the substrate-specificity of ACs. Sixth, a systematic analysis of the activity-dependence of AC inhibitors is required, aiming at the identification of compounds that selectively inhibit pathologically high enzyme activity while leaving unaffected physiologically relevant catalysis. Seventh, our studies will facilitate the analysis of the interaction of diterpenes with AC. Diterpenes interact with AC according to a two-step model [46]. In the first step, diterpenes bind to AC, and in the second step, they induce or stabilize a conformational change that initiates catalysis. To this end, the analysis of conformational changes in AC by diterpenes has only been conducted with MANT-GTP as fluorescence sensor [46]. However, MANT-GTP is not the most sensitive sensor in this regard, and is clearly surpassed by ANT-GTP for the analysis of direct fluorescence changes and 2'-d-3'-MANT-GTP for FRET (compare Fig. 2F and N and Fig. 4I). Moreover, 3'-d-2'-MANT-ATP provides a novel probe to monitor inhibitory effects of diterpenes on the nucleotides bound to VC1:IIC2 (Fig. 4G and H). These studies will also help us understand mechanisms of AC regulation in more general terms. Lastly, concerning future design of both inhibitors and activators for ACs, much can be learned from the analysis of G-protein-coupled receptors. Specifically, much evidence has been accumulated in favor of the existence of

complex conformational landscapes that are being modulated in a ligand-specific manner by orthosteric and allosteric ligands, resulting highly complex signal transduction outcomes [47–50].

All in all, the fields of ligand design for G-protein-coupled receptors and ACs, having developed as completely separate entities for a long time, could be merged, perhaps even with receptors modulating the pharmacological properties of ACs and *vice versa*. Recently, we have identified inhibitors with a 100-fold selectivity for the bacterial AC toxin CyaA from *Bordetella pertussis* relative to mammalian ACs [41]. These data show that in principle, it is possible to obtain isoform-selective AC inhibitors. Ultimately, this is the long-term goal of our research program.

#### Acknowledgments

This work was supported by Deutsche Forschungsgemeinschaft research grant Se 529/5-2 to R.S. and NIH grant 2R56 DK46371-14 to S.R.S. Thanks are due to the reviewers for their helpful critique.

#### References

- [1] Sunahara RK, Dessauer CW, Gilman AG. Complexity and diversity of mammalian adenylyl cyclases. *Annu Rev Pharmacol Toxicol* 1996;36:461–80.
- [2] Hanoune J, Defer N. Regulation and role of adenylyl cyclase isoforms. *Annu Rev Pharmacol Toxicol* 2001;41:145–74.
- [3] Tang WJ, Hurley JH. Catalytic mechanism and regulation of mammalian adenylyl cyclases. *Mol Pharmacol* 1998;54:231–40.
- [4] Pinto C, Papa D, Hübner M, Mou TC, Lushington GH, Seifert R. Activation and inhibition of adenylyl cyclase isoforms by forskolin analogs. *J Pharmacol Exp Ther* 2008;325:27–36.
- [5] Sadana R, Dessauer CW. Physiological roles for G protein-regulated adenylyl cyclase isoforms: insights from knockout and overexpression studies. *Neurosignals* 2009;17:5–22.
- [6] Wang H, Gong B, Vadakkan KI, Toyoda H, Kaang BK, Zhuo M. Genetic evidence for adenylyl cyclase 1 as a target for preventing neuronal excitotoxicity mediated by N-methyl-D-aspartate receptors. *J Biol Chem* 2007;282:1507–17.
- [7] Watts VJ. Adenylyl cyclase isoforms as novel therapeutic targets: an exciting example of excitotoxicity neuroprotection. *Mol Interv* 2007;7:70–3.
- [8] Chester JA, Watts VJ. Adenylyl cyclase 5: a new clue in the search for the “fountain of youth”? *Sci STKE* 2007;413:pe64.
- [9] Okumura S, Takagi G, Kawabe J, Yang G, Lee MC, Hong C, et al. Disruption of type 5 adenylyl cyclase gene preserves cardiac function against pressure overload. *Proc Natl Acad Sci USA* 2003;100:9986–90.
- [10] Kim KS, Kim J, Back SK, Im JY, Na HS, Han PL. Markedly attenuated acute and chronic pain responses in mice lacking adenylyl cyclase-5. *Genes Brain Behav* 2007;6:120–7.
- [11] Yan L, Vatner DE, O'Connor JP, Ivessa A, Ge H, Chen W, et al. Type 5 adenylyl cyclase disruption increases longevity and protects against stress. *Cell* 2007;130:247–58.
- [12] Rottländer D, Matthes J, Vatner SF, Seifert R, Herzog S. Functional adenylyl cyclase inhibition in murine cardiomyocytes by 2'-(3')-O-(N-methylanthraniloyl)-guanosine 5'-[γ-thio]triphosphate. *J Pharmacol Exp Ther* 2007;321:608–15.
- [13] Gille A, Seifert R. 2'-(3')-O-(N-Methylanthraniloyl)-substituted GTP analogs: a novel class of potent competitive adenylyl cyclase inhibitors. *J Biol Chem* 2003;278:12672–9.
- [14] Gille A, Lushington GH, Mou TC, Doughty MB, Johnson RA, Seifert R. Differential inhibition of adenylyl cyclase isoforms and soluble guanylyl cyclase by purine and pyrimidine nucleotides. *J Biol Chem* 2004;279:19955–69.
- [15] Jameson DM, Eccleston JF. Fluorescent nucleotide analogs: synthesis and applications. *Methods Enzymol* 1997;278:363–90.
- [16] Mou TC, Gille A, Fancy DA, Seifert R, Sprang SR. Structural basis for the inhibition of mammalian membrane adenylyl cyclase by 2'-(3')-O-(N-methylanthraniloyl)-guanosine 5'-triphosphate. *J Biol Chem* 2005;280:7253–61.
- [17] Mou TC, Gille A, Suryanarayana S, Richter M, Seifert R, Sprang SR. Broad specificity of mammalian adenylyl cyclase for interaction with 2',3'-substituted purine- and pyrimidine nucleotide inhibitors. *Mol Pharmacol* 2006;70:878–86.
- [18] Gille A, Guo J, Mou TC, Doughty MB, Lushington GH, Seifert R. Differential interactions of G-proteins and adenylyl cyclase with nucleoside 5'-triphosphates, nucleoside 5'-[γ-thio]triphosphates and nucleoside 5'-[β,γ-imido]triphosphates. *Biochem Pharmacol* 2005;71:89–97.
- [19] Wang JL, Guo J-X, Zhang Q-Y, Wu J-Q, Seifert R, Lushington GH. A Conformational transition in the adenylyl cyclase catalytic site yields different binding modes for ribosyl-modified and unmodified nucleotide inhibitors. *Bioorg Med Chem* 2007;15:2993–3002.
- [20] Suryanarayana S, Göttle M, Hübner M, Gille A, Mou TC, Sprang SR, et al. Differential inhibition of various adenylyl cyclase isoforms and soluble guanylyl cyclase by 2',3'-O-(2,4,6-trinitrophenyl)-substituted nucleoside 5'-triphosphates. *J Pharmacol Exp Ther* 2009;330:687–95.

- [21] Göttle M, Geduhn J, König B, Gille A, Höcherl K, Seifert R. Characterization of mouse heart adenylyl cyclase. *J Pharmacol Exp Ther* 2009;329:1156–65.
- [22] Suryanarayana S, Pinto C, Mou TC, Richter M, Lushington GH, Seifert R. The C1 homodimer of adenylyl cyclase binds nucleotides with high affinity but possess exceedingly low catalytic activity. *Neurosci Lett* 2009;467:1–5.
- [23] Hübner M, Mou TC, Lushington GH, Pinto C, Gille A, Geduhn J, König B, Sprang SR, Seifert R. Structural basis for the high-affinity inhibition of mammalian adenylyl cyclase by 2',3'-O-(N-methylanthraniloyl)-inosine 5'-triphosphate. *Mol Pharmacol*; in press.
- [24] Suryanarayana S, Wang JL, Richter M, Shen Y, Tang WJ, Lushington GH, et al. Distinct interactions of 2'- and 3'-O-(N-methyl)anthraniloyl-isomers of ATP and GTP with the adenylyl cyclase toxin of *Bacillus anthracis*, edema factor. *Biochem Pharmacol* 2009;78:224–30.
- [25] Hiratsuka T. New ribose-modified fluorescent analogs of adenine and guanine nucleotides available as substrates for various enzymes. *Biochim Biophys Acta* 1983;742:496–508.
- [26] Göttle M, Dove S, Steindel P, Shen Y, Tang WJ, Geduhn J, et al. Molecular analysis of the interaction of *Bordetella pertussis* adenylyl cyclase with fluorescent nucleotides. *Mol Pharmacol* 2007;72:526–35.
- [27] Taha H, Schmidt J, Göttle M, Suryanarayana S, Shen Y, Tang WJ, et al. Molecular analysis of the interaction of anthrax adenylyl cyclase toxin, edema factor, with 2'(3')-O-(N-(methyl)anthraniloyl)-substituted purine and pyrimidine nucleotides. *Mol Pharmacol* 2009;75:693–703.
- [28] Sunahara RK, Dessauer CW, Whisnant RE, Kleuss C, Gilman AG. Interaction of  $G_{s\alpha}$  with the cytosolic domains of mammalian adenylyl cyclase. *J Biol Chem* 1987;262:22265–71.
- [29] Seifert R, Lee TW, Lam VT, Kobilka BK. Reconstitution of  $\beta_2$ -adrenoceptor-GTP-binding-protein interactions in Sf9 cells: High coupling efficiency in a  $\beta_2$ -adrenoceptor- $G_{s\alpha}$  fusion protein. *Eur J Biochem* 1998;255:369–82.
- [30] SYBYL 8.0, The Tripos Associates, St. Louis, MO, USA, 2008.
- [31] Gasteiger J, Marsili M. A new model for calculating atomic charges in molecules. *Tetrahedron* 1978;36:3219–28.
- [32] Morris GM, Goodsell DS, Halliday RS, Huey R, Hart WE, Belew RK, et al. Automated docking using a Lamarckian genetic algorithm and empirical binding free energy function. *J Comput Chem* 1998;19:1639–62.
- [33] Gasteiger J, Marsili M. A new model for calculating atomic charges in molecules. *Tetrahedron Lett* 1978;34:3181–4.
- [34] Clark M, Cramer RD, Van Opdenbosch III N. Validation of the general purpose Tripos 5.2 force field. *J Comp Chem* 1989;10:982–1012.
- [35] Tesmer JJ, Sunahara RK, Gilman AG, Sprang SR. Crystal structure of the catalytic domains of adenylyl cyclase in a complex with  $G_{s\alpha}$ -GTP $\gamma$ S. *Science* 1997;278:1907–16.
- [36] Marti-Renom MA, Stuart AC, Fiser A, Sanchez R, Melo F, Sali A. Comparative protein structure modeling of genes and genomes. *Annu Rev Biophys Biomol Struct* 2000;29:291–325.
- [37] Thompson JD, Higgins DG, Gibson TJ. CLUSTAL W: improving the sensitivity of progressive multiple sequence alignment through sequence weighting, position-specific gap penalties and weight matrix choice. *Nucleic Acids Res* 1994;22:4673–80.
- [38] Henikoff S, Henikoff JG. Performance evaluation of amino acid substitution matrices. *Proteins* 1993;17:49–61.
- [39] Higashijima T, Ferguson KM, Sternweis PC, Ross EM, Smigel MD, Gilman AG. The effects of activating ligands on the intrinsic fluorescence of guanine nucleotide-binding regulatory proteins. *J Biol Chem* 1987;262:752–6.
- [40] Lan KL, Remmers AE, Neubig RR. Roles of  $G_{o\alpha}$  tryptophans in GTP hydrolysis, GDP release, and fluorescence signals. *Biochemistry* 1998;37:837–43.
- [41] Geduhn J, Dove S, Shen Y, Tang WJ, König B, Seifert R. Bis-halogen-anthraniloyl-substituted nucleoside 5'-triphosphates as potent and selective inhibitors of *Bordetella pertussis* adenylyl cyclase toxin. *J Pharmacol Exp Ther* 2011;336:104–15.
- [42] Zhang G, Liu Y, Ruoho AR, Hurley JH. Structure of the adenylyl cyclase catalytic core. *Nature* 1997;386:247–53.
- [43] Pieroni JP, Harry A, Chen J, Jacobowitz O, Magnusson RP, Iyengar R. Distinct characteristics of the basal activities of adenylyl cyclases 2 and 6. *J Biol Chem* 1995;270:1368–73.
- [44] Laux WH, Pande P, Shoshani I, Gao J, Boudou-Vivet V, Gosselin G, et al. Pro-nucleotide inhibitors of adenylyl cyclases in intact cells. *J Biol Chem* 2004;279:13317–32.
- [45] Göttle M, Dove S, Kees F, Schlossmann J, Geduhn J, König B, et al. Cytidylyl and uridylyl cyclase activity of *Bacillus anthracis* edema factor and *Bordetella pertussis* CyaA. *Biochemistry* 2010;49:5494–503.
- [46] Pinto C, Hübner M, Gille A, Richter M, Mou TC, Sprang SR, et al. Differential interactions of the catalytic subunits of adenylyl cyclase with forskolin analogs. *Biochem Pharmacol* 2009;78:62–9.
- [47] Kobilka BK, Deupi X. Conformational complexity of G-protein-coupled receptors. *Trends Pharmacol Sci* 2007;28:397–406.
- [48] Galandrin S, Oligny-Longré G, Bouvier M. The evasive nature of drug efficacy: implications for drug discovery. *Trends Pharmacol Sci* 2007;28:423–30.
- [49] Seifert R, Dove S. Functional selectivity of GPCR ligand stereoisomers: new pharmacological opportunities. *Mol Pharmacol* 2009;75:13–8.
- [50] Kenakin T, Miller LJ. Seven transmembrane receptors as shapeshifting proteins: the impact of allosteric modulation and functional selectivity on new drug discovery. *Pharmacol Rev* 2010;62:265–304.